I&EC research
Industrial & Engineering Chemistry Research

pubs.acs.org/IECR
Article

Amino-Acids Surfactants and *n*-Octanol Mixtures—Sustainable, Efficient, and Dynamically Triggered Foaming Systems

Mariusz Borkowski, Piotr Batys, Oleg M. Demchuk, Przemyslaw B. Kowalczuk,* and Jan Zawala*

Cite This: *Ind. Eng. Chem. Res.* 2023, 62, 13498−13509

ABSTRACT: Surfactants with amino-acid heads (AASs), namely *N*-lauroyl-L-alanine (C_{12}-ALA), *N*-lauroyl-L-leucine (C_{12}-LEU), and *N*-lauroyl-L phenylalanine (C_{12}-PHE) were mixed with *n*-octanol (C_8OH) and thoroughly investigated via surface tension and foamability experiments. Significant differences between the selected AAS were observed. Moreover, the results obtained under equilibrium and dynamic conditions were remarkably different in terms of surface activity. The surface tension measurements (equilibrium conditions) indicated that the C_{12}-ALA/C_8OH mixture exhibits the highest synergistic effect. For the C_{12}-LEU/C_8OH system, a moderate synergism was observed, while for C_{12}-PHE/C_8OH, the effect was antagonistic. In contrast, in foamability experiments (dynamic conditions), all of the studied AAS/C_8OH mixtures exhibited a spectacular synergistic effect at a wide concentration range. The observed effect was referred to as convection-activated surface activity of AAS/C_8OH mixtures. The obtained experimental results were interpreted on the molecular level via all-atom detail molecular dynamics simulations (MD). The observed phenomenon was connected with the hydrogen bond-mediated aggregate formation in the bulk solution. Such aggregates act as reservoirs of surfactant molecules for supplementation of the adsorption coverage at the freshly formed liquid/gas interface. Additionally, the differences between the specific AAS were explained via the interplay of AAS−AAS and AAS-C_8OH hydrogen bond affinities. The presented results showed an interesting example of a foaming system in which the surface activity can be controlled in situ via convection. This finding also significantly expands the range of potentially interesting molecules that can be used as efficient foaming additives and impacts the current understanding of the role of hydrogen bonding in designing of tuneable surfactant mixtures.

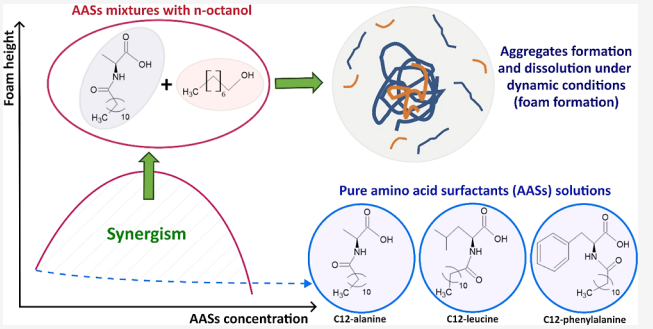

1. INTRODUCTION

Surfactants, also known as surface-active substances (SAS), are a group of compounds with unique properties (e.g., the ability to lower the surface tension) that make them incredibly versatile and useful in a wide range of industrial, technological, and everyday human life applications. Some of the common applications of surfactants are emulsification, corrosion inhibition, wetting, foaming, cleaning, dispersing, and so on.[1−7] However, traditional surfactants are often derived from petroleum or other non-renewable sources and might have a negative impact on the environment and human life.[8] Therefore, there is a growing interest in the potential replacement of toxic petroleum-based surfactants by developing more sustainable surfactant formulations that can meet the needs of various industries while reducing the environmental impact (i.e., green surfactants).[6,8−12]

One of the promising approaches to achieving more sustainable surfactant formulations is the use of mixed surfactants.[13−19] Mixing of two or more different types of surfactants often demonstrates improved surface activity.[20−22] Such systems can exhibit synergistic effects that improve their performance, reduce consumption, and thus minimize waste generation.

However, despite the potential benefits of mixed surfactants, there are also several challenges associated with their use. For example, mixed surfactants can be difficult to synthesize, stabilize, and use effectively in various processes as they can form crystalline precipitates in aqueous solutions.[23−25] In addition, there are often trade-offs between the different properties of mixed surfactants and blends compositions, making it challenging to optimize their use for different applications.[26,27] Therefore, it is important to carefully consider the potential benefits and challenges of mixed surfactants when exploring their use in various applications.

Received: June 12, 2023
Revised: July 25, 2023
Accepted: July 27, 2023
Published: August 17, 2023

https://doi.org/10.1021/acs.iecr.3c01972
Ind. Eng. Chem. Res. 2023, 62, 13498−13509

There is a large body of literature on the use of mixed surfactants; however, to the best of the authors' knowledge, no studies have been reported in the literature on the foaming properties of amino-acid surfactants (AASs) mixed with fatty alcohols. AASs are derived from natural amino acids and have a vast number of unique properties (e.g., mildness, biodegradability, low toxicity, good foaming, and stability over wide range of pH) that make them competitive with typical surface-active substances.[2,28−30] One of the key advantages of fatty alcohols is their biodegradability and low toxicity. They can be derived from renewable resources, such as vegetable oils and animal fats, which also makes them a more sustainable alternative to synthetic chemicals.

In this paper, we investigated the foaming properties of three AASs with different hydrophilic heads (amino acids), namely, *N*-lauroyl-L-alanine (C_{12}-ALA), *N*-lauroyl-L-leucine (C_{12}-LEU), and *N*-lauroyl-L phenylalanine (C_{12}-PHE), mixed with *n*-octanol (C_8OH) which is a simple fatty alcohol. First, we examined how the surfactants' type and dose change the surface tension and foamability of the mixed surfactants. Second, we performed MD simulations of the corresponding systems to analyze and understand the phenomenon on the molecular level. Third, we assessed how surfactant dose affected aggregate formation in the bulk of the mixed surfactant systems. Finally, we explained the quite unexpected discrepancy between equilibrium surface tension variations and foamability of mixed AASs/fatty alcohol solutions, defining the so-called convection-induced surface activity, directly related to the bulk aggregation phenomenon.

2. MATERIALS AND METHODS

2.1. Materials. All experiments were carried out in an aqueous solution of the AASs, whose synthesis pathways and detailed adsorption characteristics at the air/solution interface (including molecular dynamic simulations, DFT calculations, and derivation of the adsorption isotherm equation) were presented elsewhere.[31] To study the effect of non-ionic surfactant addition on the AASs solutions' foamability (i.e., foam height and stability), the experiments involved pure AASs solutions as well as blends of AASs with constant amounts of *n*-octanol (simple fatty alcohol with eight carbon atoms in the hydrophobic chain, C_8OH, see Figure 1D). Three AASs with different hydrophilic heads (amino acids), namely, *N*-lauroyl-L-alanine (C_{12}-ALA), *N*-lauroyl-L-leucine (C_{12}-LEU), and *N*-lauroyl-L phenylalanine (C_{12}-PHE), whose structures are shown in Figure 1, were chosen in this study. The AASs were synthesized by the condensation of a proper amino acid with dodecanoyl (lauroyl) chloride, obtained from the reaction of lauric acid with thionyl chloride. The detailed description of the AASs synthesis pathway, their purity analysis, and the crystal structures can be found elsewhere.[31,32] C_8OH (purity > 98%) was purchased from Merck. In two-component solutions, concentration of the chosen AAS, as the solution main component, was changed in a quite broad range, while the concentration of C_8OH (non-ionic additive) was kept constant and equal to either 1×10^{-4} or 5×10^{-4} mol/dm^3.

All solutions used in this study were prepared in ultrapure water (Direct-Q3 UV Water Purification System by Millipore, conductivity < 0.7 μS/cm, surface tension equal to 72.6 mN/m, and temperature equal to 22 ± 1 °C).

Before each experimental series, all glass parts of the laboratory equipment used for solutions preparation and physicochemical tests were washed with a diluted solution of Mucasol−Schülke (commercially available laboratory cleaning liquid) purchased from Sigma-Aldrich and then rinsed thoroughly with a large amount of Milli-Q water.

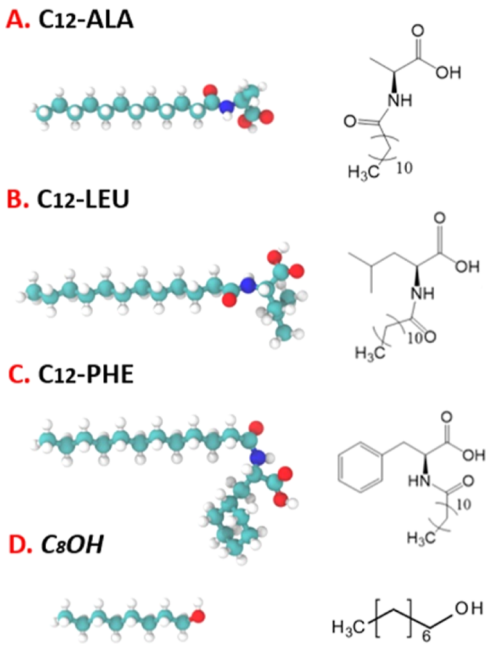

Figure 1. Chemical structure of (A) *N*-lauroyl-L-alanine (C_{12}-ALA), (B) *N*-lauroyl-L-leucine (C_{12}-LEU), (C) *N*-lauroyl-L phenylalanine (C_{12}-PHE), and (D) *n*-octanol (C_8OH).

2.2. Equilibrium Surface Tension Measurements. The equilibrium values of the surface tension for all tested systems (either pure or blended AASs/C_8OH solutions) were determined using a bubble shape method using a PAT-1 tensiometer (SINTERFACE Technologies, Berlin, Germany) with an automatic bubble volume correction algorithm. In these experiments, the surface tension values were determined by analyzing the shape of a submerged bubble attached to a U-shaped needle immersed in a quartz cuvette (25 mL) filled with the studied solution. The estimation of the surface tension was achieved by fitting the Young−Laplace equation to the bubble outline (acquired by a CCD camera) as a function of time. For all experiments, the surface tension was measured for 1 h, and the equilibrium surface tension values were calculated accordingly from the period, where the surface tension values started to be constant in time. All surface tension measurements were carried out at room temperature (22 ± 1 °C).

2.3. Foamability. Foamability and foam stability of pure AASs solutions of various concentrations, as well as their blends with constant C_8OH concentration, were assessed using a Dynamic Foam Analyzer (DFA100, KRÜSS GmbH) apparatus. The apparatus consisted of (i) a cylindrical column, (ii) two parallel electrodes with seven sensors to measure the foam liquid fraction at different heights, and (iii) two vertical rows of photodiodes as light sources (blue—λ = 469 mm) and light scanners for simultaneous automatic measurement of foam (H_f) and solution (H_s) heights as a function of time. The filter paper made of chemically pure cellulose with pore sizes equal to 12−15 μm, mounted at the bottom of the column, was used as an air disperser. In all foaming tests, after mounting the filter paper at the column bottom, the column was placed on the DFA100 stand and filled with 60 mL of the studied solution. The air was pumped through the disperser at

https://doi.org/10.1021/acs.iecr.3c01972
Ind. Eng. Chem. Res. 2023, 62, 13498−13509

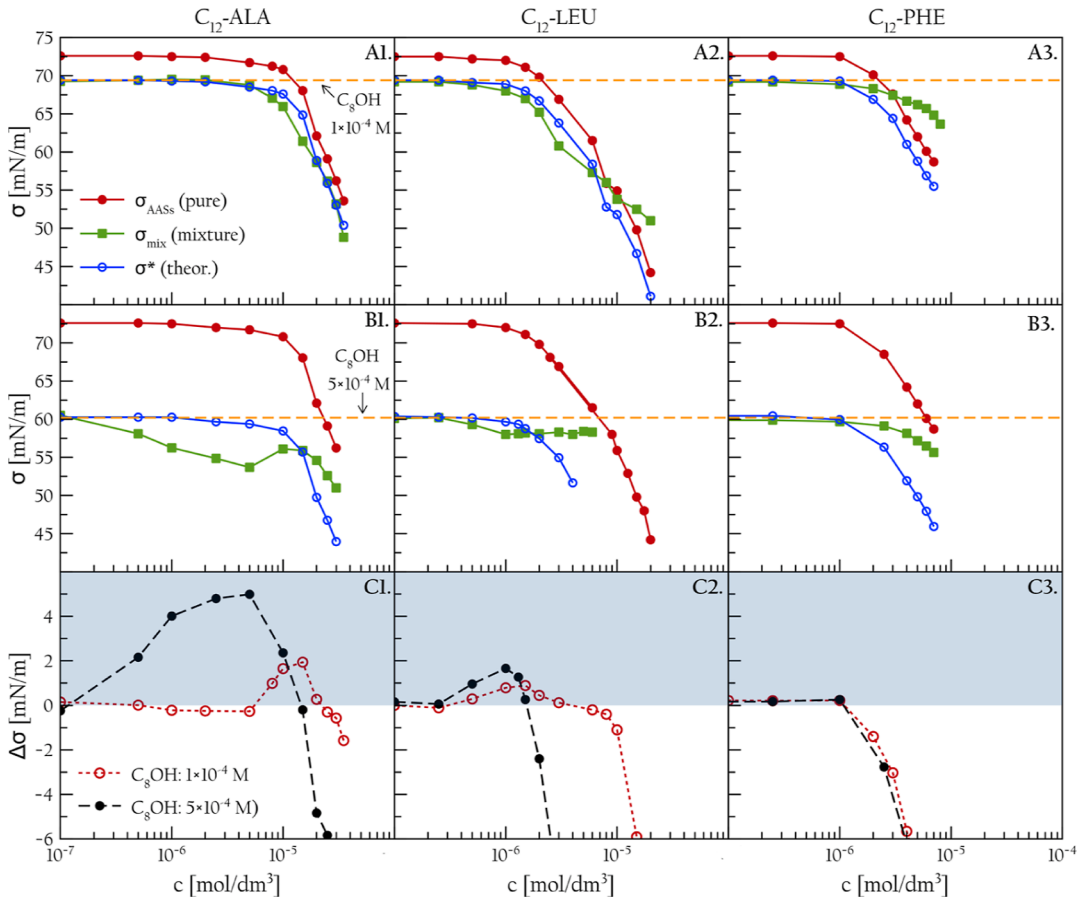

Figure 2. Data on surface tension of AASs solutions, either pure (full red circles) or mixed (green full squares) with two chosen C_8OH concentrations (1×10^{-4}—first row and 5×10^{-4} mol/dm^3—second row, with σ marked as horizontal dashed lines). The third row shows the data on $\Delta\sigma$, calculated according to eq 3.

a flow rate of 0.5 L/min for 60 s, and the H_f and H_s time evolutions, as well as the foam liquid content, were recorded by a PC, employing the ADVANCE software (KRÜSS GmbH). The experiments were carried out at room temperature (22 ± 1 °C).

2.4. Dynamic Light Scattering. Aggregation dynamics and aggregates' hydrodynamic radii were monitored by the dynamic light scattering (DLS) method in a Zetasizer ZS Malvern ZEN 3500 apparatus (with a laser of wavelength 532 nm). The measurements were conducted with the use of standard DLS quartz cuvettes. At least 10 independent runs for the aggregate size distribution determination in all prepared mixed AASs/C_8OH solutions were performed (count rate) in the time range of 36 min, with a time resolution equal to 4 min. Fresh solutions were used in these studies immediately after their preparation (by mixing the proper amounts of pure AASs and pure C_8OH solutions at proper concentrations). Blank tests, consisting of measurements of hydrodynamic radii of aggregates, which could be potentially formed in the one-component AASs and pure C_8OH solutions of concentrations corresponding to the concentrations used later in the mixtures, were also carried out. As discussed later, the blank tests did not reveal any aggregates' presence in the pure solutions.

2.5. Molecular Dynamics Simulations. The Gromacs 2019.2 package,[33,34] with the CHARMM[35] force field, was used for all-atom molecular dynamics (MD) simulations. The system setup and parameters were adapted from Yazhgur et al.[36] The structure and topology of AASs were generated using the CHARMM-GUI web server.[37−39] For C_8OH, the compatible CHARMM general force field was used.[40] For water, the modified TIP3P model of CHARMM was applied.[35,41] To make the simulation systems charge neutral, an adequate number of Br- ions was added. After 200 steps of energy minimization, the systems were simulated for 70 ns, while the first 20 ns were considered the initial equilibration period and disregarded from the analysis.

All MD simulations were run under constant temperature and volume (*NVT* ensemble) conditions. Temperature coupling was controlled via a V-rescale thermostat[42] at a temperature of 298 K and a coupling constant of 0.5 ps. Van der Waals interactions were described by the Lennard-Jones potential, which smoothly shifted to zero between 1.0 and 1.2 nm. The electrostatic interactions were modeled by the PME method,[43] corrected for the slab geometry,[44] with a 1.2 nm cut-off, 0.12 nm grid spacing, and fourth-order splines. Equations of motion were integrated using a leap-frog integration scheme and a 2 fs time step. Bonds involving hydrogen were constrained using the LINCS[45] and SETTLE[46] algorithms. All molecular visualizations employed the VMD software package.[47]

For the simulations, a periodic rectangular simulation box, 8 × 8 × 24 nm^3, consisting of an ∼8 nm thick water slab, separated by a vacuum region, was used. Initial configurations were generated using PACKMOL.[48] Monolayers were constructed by randomly placing surfactant molecules into two monolayers at opposite orientations. Surfactant head-

https://doi.org/10.1021/acs.iecr.3c01972
Ind. Eng. Chem. Res. 2023, 62, 13498−13509

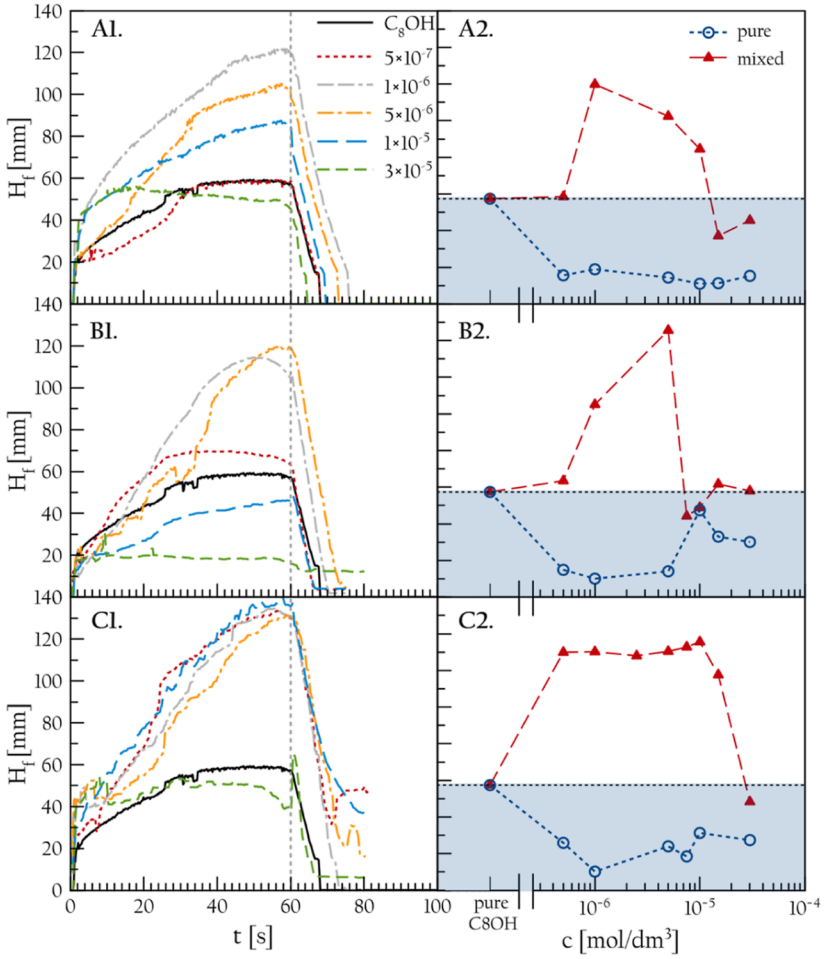

Figure 3. Height of the foam (H_f) as function of time (1) measured for C_8OH (5×10^{-4} mol/dm^3) mixed AASs/C_8OH solutions, and the maximum foam height both for pure and mixed systems after 60 s of gas supply (2) for (A) C_{12}-ALA, (B) C_{12}-LEU, and (C) C_{12}-PHE. In the case of (1), the data for AASs/C_8OH (5×10^{-4} mol/dm^3) mixed solutions are presented. For (2), both pure (hollow squares) and mixed systems (red triangles) are shown (data of figure are available in the open repository—https://doi.org/10.18150/CLCRGT).

groups were oriented toward the water slab, while the angle between the tail and the interface was chosen randomly. Amounts of surfactants on the surface were calculated based on their bulk concentration in pure one-component solutions, according to ref 31. In the case of surfactant mixtures, where their exact surface concentrations were not known experimentally, a simple addition was used as the initial approach.

3. RESULTS

3.1. Equilibrium Surface Tension Results. The data on equilibrium surface tension (σ) as a function of the AAS solution concentrations with and without C_8OH addition are presented in Figure 2. The experimental data for pure AASs solutions are given as full red circles. The corresponding experimental data for the two-component systems (σ_{mix}) are shown as full squares (first row of Figure 2, A1−A3, for AASs/C_8OH blends with a constant C_8OH concentration equal to 1×10^{-4} mol/dm^3; second row, B1−B3, for AASs/C_8OH blends with a constant C_8OH concentration equal to 5×10^{-4} mol/dm^3). For each data set, the σ values of pure C_8OH solutions of two chosen concentrations ($\sigma_{C_8OH}^{1\times10^{-4}} = 69.4 \pm 0.3$ and $\sigma_{C_8OH}^{5\times10^{-4}} = 60.2 \pm 0.1$ mN/m) are given in the corresponding figures as horizontal dashed lines. The third dependence presented in the first two rows of Figure 2 as blue hollow circles illustrates the theoretical surface tension values (σ^*), which would result from the simple summation of the effect of the decrease of surface tension of pure AASs solutions (σ_{AASs}) caused only by the C_8OH addition (with respect to water). The values of σ^* were calculated as

$$\sigma_{H_2O} - \sigma^* = [\sigma_{H_2O} - \sigma_{AASs}(c)] + [\sigma_{H_2O} - \sigma_{C_8OH}^{1\times10^{-4}}] \quad (1)$$

$$\sigma_{H_2O} - \sigma^* = [\sigma_{H_2O} - \sigma_{AASs}(c)] + [\sigma_{H_2O} - \sigma_{C_8OH}^{5\times10^{-4}}] \quad (2)$$

where σ_{H_2O} was taken as 72.6 mN/m.

As seen in Figure 2, addition of C_8OH significantly reduced the AAS solution surface tension, and obviously, this effect is higher for higher concentrations of the non-ionic additive in all studied cases. This surface tension drop, especially for small AAS concentrations, is obvious and was expected as a consequence of a C_8OH molecule excess in the solution.

It can be noticed, however, that the course of the theoretical surface tension values' (σ^*) variations for higher AASs concentrations shows significant discrepancies in comparison to values obtained experimentally for mixed solutions (presented in Figure 2 as green squares). This phenomenon, much smaller and almost negligible in the case of $c_{C_8OH} = 1 \times 10^{-4}$ mol/dm^3, can be very well distinguished for higher C_8OH concentrations (5×10^{-4} mol/dm^3). Although this effect is

https://doi.org/10.1021/acs.iecr.3c01972
Ind. Eng. Chem. Res. 2023, 62, 13498−13509

clearly visible, its magnitude and direction strictly depend on the type of amino acid in the AASs headgroup. As was previously proposed in ref 16, to visualize this effect, the value of $\Delta\sigma$ can be compared for both pure and mixed systems. According to this concept, for all studied AASs, the values of $\Delta\sigma$ were calculated as

$$\Delta\sigma = \sigma^* - \sigma_{mix} \quad (3)$$

The values of $\Delta\sigma$ are presented in the last row of Figure 2 (C1−C3) for both C_8OH concentrations studied. The physical meaning of the $\Delta\sigma$, after the discussion presented in ref 16, can be interpreted as follows:

- if $\Delta\sigma = 0$, the non-ionic additive (C_8OH) has no effect in the observed variations of the AASs solution surface tension,
- if $\Delta\sigma > 0$, the effect of the solution surface tension decrease is higher than could be expected, indicating the existence of the so-called synergistic effect,
- if $\Delta\sigma < 0$, the solution surface tension decrease is weaker than could be expected, indicating the existence of the so-called antagonistic effect.

The $\Delta\sigma$ analysis performed for cationic/non-ionic binary mixtures of classical surfactants can be used as a very convenient tool for fast and simple estimation of synergistic effect concentration ranges and values of the so-called critical synergistic concentration (CSC), i.e., the maximum concentration for which the synergistic effect is no longer visible (when $\Delta\sigma$ starts to be negative or equal zero). It was shown that the CSC values calculated from $\Delta\sigma$ analysis (CSC_σ) agreed perfectly with the CSC calculated from trends observed in variations of the solutions foamability (CSC_{DFA}) and can be used as a predictor of this important quantity.

As seen in Figure 2C, for the studied system of mixed surfactants, $\Delta\sigma = 0$ can be noticed only for small AASs concentrations. For C_{12}-ALA and C_{12}-LEU in some specific concentration ranges, $\Delta\sigma$ starts to be greater than zero, indicating the existence of a synergistic effect. As a result, the mixed components interact in some specific manner at the air/solution interface, and, as a consequence, the overall surface concentration is higher compared to that of a pure AASs mixture, and the surface tension decrease is strengthened. This effect is much more pronounced for C_{12}-ALA (Figure 2C1) and a higher concentration of C_8OH. For mixed C_{12}-ALA and C_8OH ($c_{C_8OH} = 1 \times 10^{-4}$ mol/dm^3), the synergistic effect is smaller, and its starting point is significantly shifted toward a higher concentration. For C_{12}-LEU, the synergistic effect is similar for both studied c_{C_8OH} with only a slight concentration shift. It can be noticed that for both C_{12}-ALA and C_{12}-LEU, when some specific AASs concentration is exceeded, the synergistic effect disappears. As it was discussed elsewhere, this concentration value corresponds to the so-called CSC.[49] In the case of the C_{12}-PHE surfactant, the overall picture is quite different. After the initial span within which $\Delta\sigma = 0$, the $\Delta\sigma$ value drops around $c_{C12\text{-}PHE} = 1 \times 10^{-6}$ mol/dm^3 and starts to be negative for both C_8OH concentrations, which indicates that the observed effect of C_8OH addition is antagonistic, instead of synergistic. Here, this effect does not depend on the concentration of C_8OH. It is worth highlighting here that both effects assessed based on the analysis of equilibrium surface tension values are rather small. For $c_{C_8OH} = 5 \times 10^{-4}$ mol/dm^3, in the case of C_{12}-ALA and C_{12}-LEU the maximum $\Delta\sigma$ value was equal to ca. 5 and 2.5 mN/m, respectively, while for C_{12}-PHE, it was ca. −8 mN/m.

3.2. Foamability and Foam Stability Analysis. Since the magnitude of either synergistic or antagonistic effects postulated based on the $\Delta\sigma$ analysis presented above was generally higher for the higher C_8OH concentration used in this study (see Figure 2), the foamability experiments were performed only for mixed solutions with $c_{C_8OH} = 5 \times 10^{-4}$ mol/dm^3. Figure 3 shows the time evolution of the foam height (H_f) in AASs/C_8OH mixed surfactant solutions (Figure 3A1−C1), as well as the maximum foam height (H_f^{max}) taken after 60 s (Figure 3A1−C2), as a function of the concentration of amino acid surfactants. The maximum foam height was read off from the moment when the air supply to the column was stopped (it is marked with a vertical dashed line in Figure 3A1−C1). In Figure 3A2,B2,C2, the full red triangles represent the data taken for mixed systems, while the hollow blue circles represent pure AASs solution. For pure AASs, the foamability was rather poor, and the H_f^{max} data for these systems (right column of Figure 3, blue circles) correspond to the maximum possible foam height registered during experiments. Furthermore, the mean liquid fraction (ϕ) measured (data not presented) was much higher than the threshold value assumed for the so-called wet (unstable) foams ($\phi > 10\%$).[50,51]

As seen for C_{12}-ALA and C_{12}-LEU solutions, a spectacular increase in foamability in the presence of C_8OH was revealed in some specific AASs concentration ranges. Compared to pure 5×10^{-4} mol/dm^3 C_8OH, the H_f^{max} in mixed surfactant systems could be even higher than twice. Keeping in mind that the foamability of pure C_{12}-ALA and C_{12}-LEU solutions was almost negligible (H_f^{max} ca. 20−30 mm), the observed effect is quite spectacular and correlates qualitatively with changes in the solution surface tension (see Figure 2). Surprisingly, for C_{12}-PHE solutions, where, according to the $\Delta\sigma$ analysis, the antagonistic effect for foamability was expected, the H_f^{max} was even higher, and the evident synergistic effect could be observed for the widest concentration range (between ca. 5×10^{-7} and 2×10^{-5} mol/dm^3). In other words, in this case, the best foamability performance was revealed. It is worth adding that, despite the significant synergistic effect related to the C_8OH presence in AASs solutions and foamability enhancement (in specific concentration ranges determined in Figure 3), the foam stability was quite low. The so-called time of deviation (t_{dev}), allowing foam stability assessment, calculated according to the procedure described in refs 49 and 50 was smaller than 1 s for all AASs surfactants studied (which is a characteristic feature of wet foams).

In contrast to the discussion presented in ref 16, in the case of mixed AASs/C_8OH systems, there is no general quantitative agreement between CSC_σ and CSC_{DFA}, the values of which, read from Figures 2 and 3, are gathered in Table 1. For C_{12}-ALA, the agreement seems to exist, but for C_{12}-LEU, the CSC_σ is smaller than CSC_{DFA} almost by an order of magnitude. For C_{12}-PHE, due to the fact that the $\Delta\sigma$ analysis suggested the existence of an antagonistic effect, the CSC_σ value could not be determined, but the CSC_{DFA} was easily distinguished.

In order to understand the mechanism of such unexpected behavior of the AASs/C_8OH mixtures on the molecular level, molecular dynamic (MD) simulations were performed to provide additional insight into the interfacial properties and adsorption layer architecture.

3.3. MD Simulations. The experiments revealed that the C_8OH addition significantly enhances the foamability of AASs

https://doi.org/10.1021/acs.iecr.3c01972
Ind. Eng. Chem. Res. 2023, 62, 13498−13509

Table 1. Values of the Critical Synergistic Concentrations Determined from Adsorption Isotherms (CSC_σ) and Foamability Tests (CSC_{DFA})

AASs	c_{C_8OH} [M]	CSC_σ [M]	CSC_{DFA} [M]
C12-ALA	1×10^{-4}	2.2×10^{-5}	
	5×10^{-4}	1.4×10^{-5}	1.3×10^{-5}
C12-LEU	1×10^{-4}	3.8×10^{-6}	
	5×10^{-4}	1.6×10^{-6}	9.3×10^{-6}
C12-PHE	1×10^{-4}	N/A	
	5×10^{-4}	N/A	2.1×10^{-5}

solutions in certain AASs concentration ranges, despite quite different adsorption performances of surfactants molecules at the solution/gas interface, assessed from the surface tension analysis. To analyze and understand this phenomenon on the molecular level, MD simulations of the corresponding systems were performed. The mixed surfactant systems, i.e., C_{12}-ALA, C_{12}-LEU, and C_{12}-PHE, with various C_8OH concentrations, were simulated at the liquid/gas interface. The changes in the surface tension as a function of the number of surfactants at the interface are presented in Figure 4. It should be mentioned that the surface tension of pure water determined for the TIP3P model is slightly different than the experimental value. Therefore, to enable comparison with experiments, the surface tensions for all systems were normalized by the value obtained

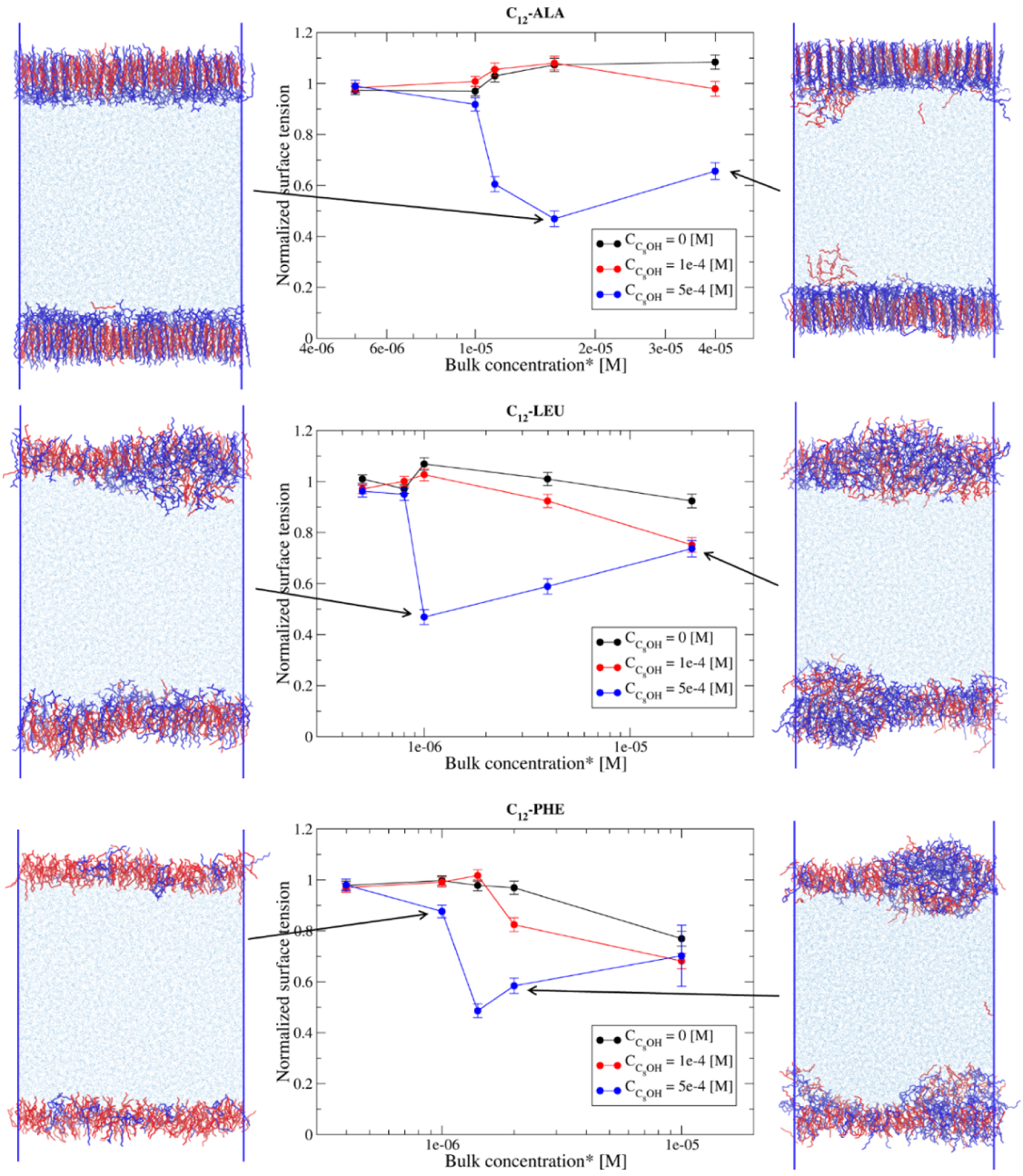

Figure 4. Normalized surface tensions for surfactants as a function of their concentration and C_8OH addition, determined from MD simulations. The snapshots correspond to the final configurations of the systems marked with arrows. In all snapshots, the C_8OH and AASs molecules are marked in red and blue, respectively.

https://doi.org/10.1021/acs.iecr.3c01972
Ind. Eng. Chem. Res. 2023, 62, 13498−13509

for TIP3P water. The snapshots presented in Figure 4 represent the final structures of the selected systems. For all studied surfactants, at the highest C_8OH concentration, the normalized surface tension exhibits a minimum. A similar effect was also observed experimentally, especially in foamability experiments. However, when comparing the MD data with the equilibrium surface tension measurements, the agreement is only visible for C_{12}-ALA. It should be noted here that the amounts of specific surfactants at the interface used in the simulations were calculated based on the molecule surface concentration measured experimentally for pure one-component solutions separately, at various bulk concentrations. In the case of surfactant mixtures, the exact amounts were not known, and simple addition was used. This can lead to some discrepancies between the simulations and experimental observations.

Nevertheless, MD simulation can provide a reasonable molecular origin of the observed synergistic effect. For pure AASs, as well as at low C_8OH concentrations, no minimum in the surface tension was observed, which agrees with the experimental data (see Figure 2). At higher C_8OH concentrations, the interface seems to be overpacked with the surfactants. In contrast to the CTAB/C_8OH mixed surfactant systems, where the increase in the number of surfactants leads to a more ordered monolayer, in the case of AASs, the surfactants tend to aggregate in micelles (see snapshots in Figure 4). For some systems, e.g., C_{12}-ALA, the micelles diffuse toward the bulk solution. The minimum in surface tension is therefore observed for the highly packed monolayers, obtained at high concentrations of C_8OH and moderate concentrations of the AASs. Further increase in the AASs concentration can induce micelle formation, and the monolayer itself becomes less organized.

To better understand the behavior of the AAS surfactants, the number of hydrogen bonds between the AAS−AAS and AAS-C_8OH in the systems with a higher C_8OH concentration was calculated. For the sake of comparison, the number of hydrogen bonds was normalized by the number of AAS molecules in the systems and plotted as a function of their surface concentration (Γ_{AAS}) (see Figure 5). As can be seen, the hydrogen bonds are present in all systems, in contrast to the previously studied CTAB/C_8OH systems. Therefore, the first conclusion, which could be drawn, is that introducing additional interactions in the system, i.e., hydrogen bonding, might disturb the surfactant ordering in the monolayer in comparison to systems without hydrogen bonds (e.g., CTAB/C_8OH). The number of hydrogen bonds formed between surfactants can also explain the differences observed between AASs with various amino acid headgroups. The AAS-C_8OH hydrogen bond formation affinity decrease is C_{12}-ALA > C_{12}-LEU > C_{12}-PHE. This reflects the interaction strength between AAS and C_8OH and therefore the stability of such mixtures at the interface. C_{12}-ALA, together with C_8OH, due to their strong hydrogen bonding interactions, can be expected to form a relatively stable interfacial monolayer. This is reflected by the equilibrium surface tension experiments via strong synergistic effect observed for C_{12}-ALA. Such effect is less pronounced in the case of C_{12}-LEU and almost disappears for C_{12}-PHE.

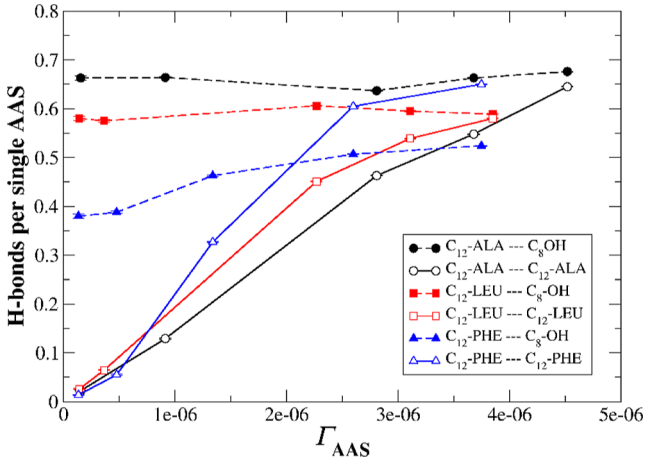

Figure 5. Number of hydrogen bonds per single AAS molecule as a function of its surface concentration (Γ_{AAS} [mol/m^2]). The C_8OH concentration equals 5×10^{-4} mol/dm^3.

Moreover, significant differences can be observed in AAS−AAS hydrogen bonding (Figure 5). The hydrogen bond formation affinity between the AAS molecules decreases as follows: C_{12}-PHE > C_{12}-LEU > C_{12}-ALA. This finding is in line with the dimerization enthalpies, previously determined for these surfactants.[31] Also, only for C_{12}-PHE, the number of AAS−AAS hydrogen bonds is larger than that of AAS-C_8OH hydrogen bonds for moderate and high surface concentrations (Γ_{AAS}). This suggests that C_{12}-PHE prefers to be surrounded by other C_{12}-PHE molecules rather than C_8OH. Therefore, its ability for micelle formation should be the strongest.

Considering the differences in hydrogen bonding as well as the observed initial micelle formation (Figure 4), one can conclude that if the micelles are present in the system, their formation will be driven by hydrogen bond interaction. Considering that C_8OH molecules do not form hydrogen bonds with themselves, one can expect that the micelles will be rich in AAS surfactants. At the same time, the interfacial layer would be AAS-depleted, where the degree of depletion would be related to the amino acid headgroup type, i.e., less depleted for C_{12}-ALA and the most depleted for C_{12}-PHE. This explains well the experimental observations from the equilibrium surface tension measurements, where the synergistic effect is visible for C_{12}-ALA but not for C_{12}-PHE.

However, it is also interesting to understand what triggers the synergistic effect during the foamability experiments. Contrary to the measured equilibrium surface tensions, the surface tensions calculated from MD simulations (Figure 4) clearly indicate that if both AAS and C_8OH molecules are present in the interfacial layer, their surface tension should decrease. Such discrepancy between the surface tensions measured experimentally and via MD can be related to the fact that the amounts of surfactants in MD simulations are fixed, so the above-mentioned depletion effect of ASS in the interfacial layer, suggested to occur in equilibrium experiments, cannot be accurately accounted for in MD. Therefore, one can expect that the foamability process itself, via constant mixing and new interface formation, enriches the interfacial layer in AAS surfactants.

Overall, based on the MD simulations results, one can conclude that under these experimental conditions, the shift in the CSC and the presence of micelles in the solution can be expected for all AASs at moderate and high bulk concentrations.

3.4. Examination of Aggregation Effect. The MD simulations suggested that addition of C_8OH can lead to aggregate formation in the bulk of the tested mixed surfactant

https://doi.org/10.1021/acs.iecr.3c01972
Ind. Eng. Chem. Res. 2023, 62, 13498−13509

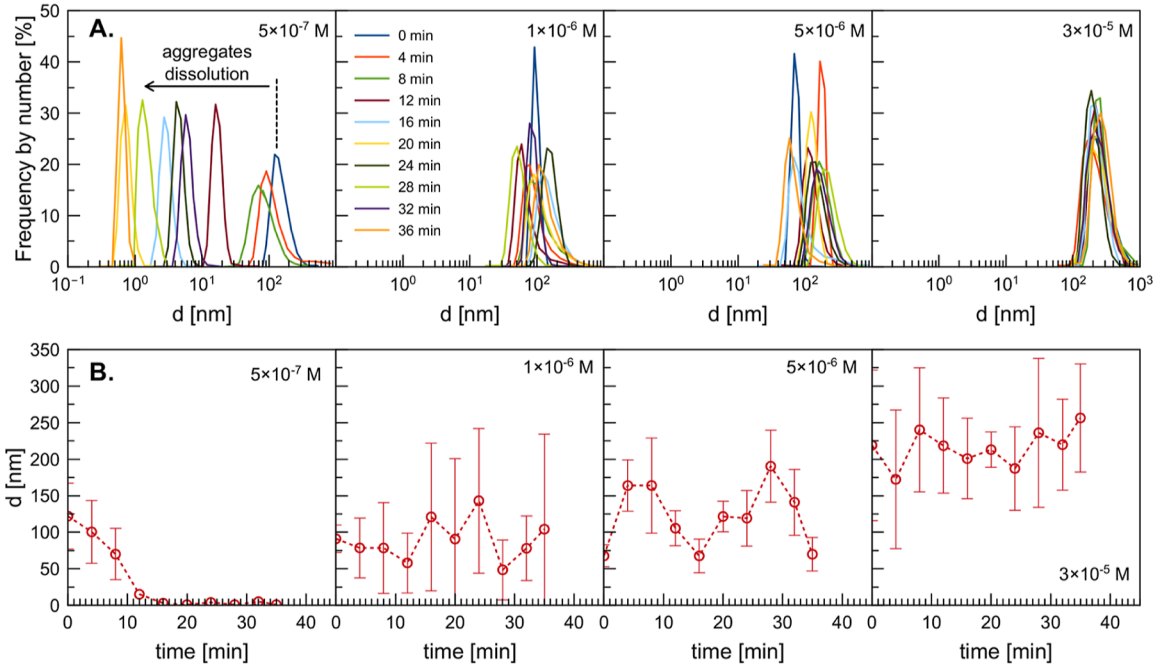

Figure 6. Distributions of the hydrodynamic diameters of the aggregates in time for C_{12}-ALA solutions of various concentrations in the presence of 5×10^{-4} mol/dm^3 C_8OH.

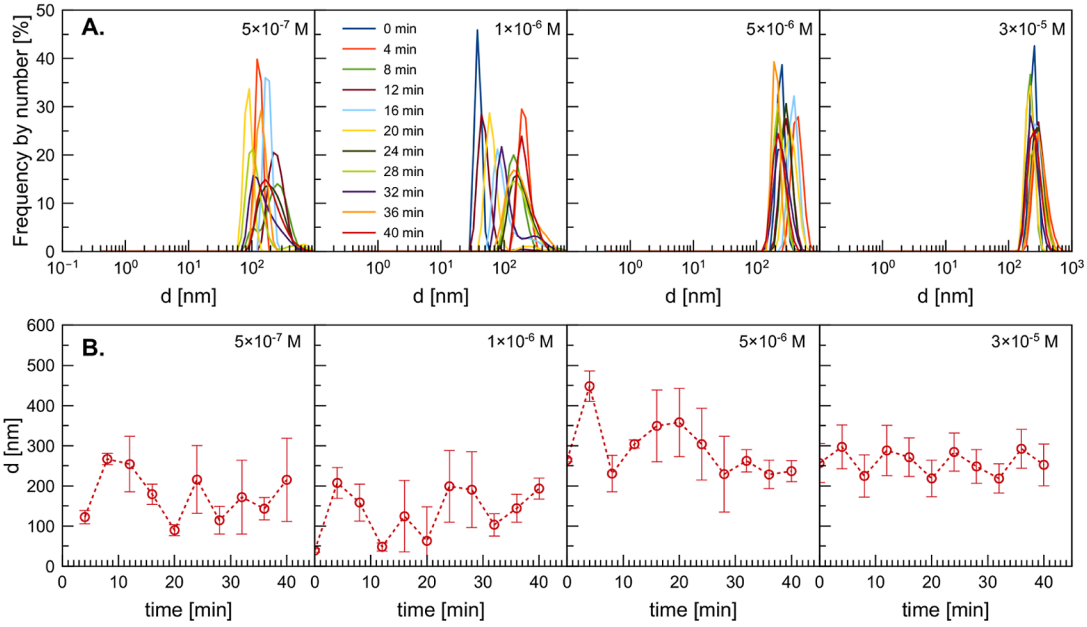

Figure 7. Distributions of the hydrodynamic diameters of the aggregates in time for C_{12}-PHE solutions of various concentrations in the presence of 5×10^{-4} mol/dm^3 C_8OH.

systems, and this effect should increase with increasing AASs concentration. To verify this assumption, dynamic light scattering (DLS) measurements were performed for selected AASs/C_8OH mixtures. Before the main experiments, blank tests were carried out using the pure solutions of C_8OH (5×10^{-4} mol/dm^3) and C_{12}-ALA (3×10^{-5} M, the highest AASs concentration measured in this study). No aggregation was observed in both cases. Next, similar experiments for mixed AASs/C_8OH solutions were performed—after mixture preparation, the DLS cuvette was immediately filled and put into the apparatus, and the hydrodynamic diameter was read at equal time intervals (every 4 min) for 36 min (this was the time corresponding to the equilibrium surface tension establishment). The results of the DLS experiments for solutions of C_{12}-ALA and C_{12}-PHE mixed with 5×10^{-4} mol/dm^3 C_8OH are presented in Figures 6 and 7, respectively.

For the C_{12}-ALA/C_8OH mixed surfactants (Figure 6), clear aggregates' presence in the bulk was revealed. As seen, for the lowest C_{12}-ALA concentration in the mixture, these aggregates were unstable—their number and diameter were gradually diminishing with time till practically complete dissolution. For the c_{AASs} equal to 1×10^{-6} and 5×10^{-6} mol/dm^3, i.e., those lying inside the range where synergistic effects were observed, only slight variations in the aggregates size could be noticed.

https://doi.org/10.1021/acs.iecr.3c01972
Ind. Eng. Chem. Res. 2023, 62, 13498−13509

For the highest concentration, aggregates were stable with time. Moreover, in the solutions with higher AASs concentration, the aggregates' mean hydrodynamic diameter increased with the concentration from 90 ± 30 nm for 1×10^{-6} mol/dm^3 and 120 ± 40 nm for 5×10^{-6} mol/dm^3 to 215 ± 25 nm for 3×10^{-5} mol/dm^3.

A similar situation can be observed for the C_{12}-PHE/C_8OH blends (Figure 7). Here, however, the aggregates were much more stable at the lowest concentration (5×10^{-7} mol/dm^3), and for $c_{C12\text{-}PHE} = 1 \times 10^{-6}$ and 5×10^{-6} mol/dm^3, only slight variations in their size could be noticed. Again, stability of the aggregates with a mean diameter of 260 ± 30 nm is the largest for $c_{C12\text{-}PHE} = 3 \times 10^{-5}$ mol/dm^3.

4. DISCUSSION

The experiments and simulations confirmed that

- the addition of C_8OH to the AASs solution, in the case of all studied AASs, induces the synergistic effect, which is quite small in the case of equilibrium surface tension variations but spectacular in the case of solution foaming performance,
- C_8OH renders the bulk aggregates formation, which does not exist in pure AASs solutions, and whose time stability depends on AASs concentration (i.e., ratio between AASs and C_8OH amount in the blend), and
- the synergistic effect for all studied AASs can be related to the formation of micelles (aggregates), which causes small surface tension variations under equilibrium conditions. Since the foam formation is highly dynamic, the aggregates are transported by convection (via constant mixing) to the freshly formed air/liquid interface.

The aggregation phenomenon explains the small and negative values of $\Delta\sigma$ calculated based on the proposed synergistic effect analysis. Excess of the AASs molecules in the bulk, in the presence of C_8OH, leads to mixed bulk micellar structures formation—the molecules cannot enter the adsorption layer because, as was shown by MD simulations, the densely packed monolayer is already formed there. The negative value of $\Delta\sigma$ revealed for the C_{12}-PHE surfactant directly shows the highest tendency of aggregation and mixed micelles formations in the case of this compound (which was confirmed by the results of MD simulations). As was shown in ref 31, the pure ASSs do not have the critical micelle concentrations (CMC) due to their solubility limit. Nevertheless, they can form intermolecular hydrogen bonds. Addition of C_8OH allows for mixed micelle formation, which results in a significant decrease in CMC.

The reason for the significant discrepancy between the synergistic effect determined based on equilibrium surface tension and solution foamability, in comparison to the results shown in our earlier studies, should be directly associated with the aggregation effect. Aggregates can act as reservoirs of AASs and *n*-octanol molecules, which, after release to the bulk and re-adsorption, cause a significantly higher (than expected) decrease in the solution surface tension due to specific interactions at the solution/air interface. In the case of solution foaming performance, the aggregates dissolution is triggered by the constant formation of new interfaces (constant and fast increase of the interfacial area)—due to the increase of the surface concentration, the surfactant bulk concentration is depleted, which disturbs the system equilibrium and shifts the aggregation constant toward release of the free surfactant molecules. In the case of low c_{AASs}, where unstable aggregates were revealed, this phenomenon exists, but most probably, the aggregates dissolution is quite fast and occurs just at the beginning of foam formation. For higher AASs concentrations, where stable aggregate formation was observed (see Figures 6 and 7), gradual depletion of the surfactant bulk concentration can be constantly re-supplied by molecules coming out from the dissolving micelle-like structures. On the other hand, due to the highly dynamic nature of the foam formation process, the aggregates can be transported to the foam layer and then adsorbed at the freshly formed air/solution interface directly from the liquid film, separating the air bubbles. The aggregates, therefore, can be considered as internal reservoirs of the mixed foaming agents, whose interactions at the interface (causing the formation of dense monolayers—see Figure 4) significantly increase the mixed solutions foamability. This effect, however, depends on the conditions rendering the aggregates stable. When the concentration of AASs/C_8OH molecules is large enough compared to the growing interfacial area (increasing interfacial area does not render significant bulk concentration depletion), the aggregates are very stable, and the foaming process does not change their stability. Furthermore, this effect can explain significantly higher CSC_{DFA} values compared to the CSC_σ—the latter (if determined based on equilibrium surface tension values) is sensitive only to the free surfactant molecules, which, in the case of proper AASs/C_8OH blends, are trapped inside the micelles.

To verify this mechanism, an additional experiment was performed. A mixed C_{12}-ALA/C_8OH solution of concentrations $1 \times 10^{-6}/5 \times 10^{-4}$ mol/dm^3, respectively, was put into the column of the DFA apparatus, and the foamability test was performed. Next, the liquid sample was taken (i) during the foam formation process (just before the H_f^{max} was reached) and (ii) after the complete foam column collapse. Next, the hydrodynamic aggregates diameter was measured in both samples (10 independent runs for each sample). It was revealed that the aggregates were bigger by ca. 30 nm in the sample taken after the foaming procedure and the foam column disappearance (see Figure 8). This experiment confirms that indeed, the aggregates can act as reservoirs of free molecules for supplementation of the adsorption coverage at the freshly formed liquid/gas interface.

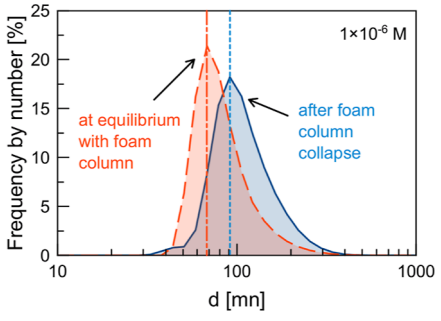

Figure 8. Aggregates diameter (d) distributions in the sample of solution taken from underneath the foam column (red) and after foam column (blue) collapse in C12-ALA solution of concentration 1×10^{-6}, mixed with 5×10^{-4} mol/dm^3 C_8OH ($\Delta d \approx 30$ nm).

https://doi.org/10.1021/acs.iecr.3c01972
Ind. Eng. Chem. Res. 2023, 62, 13498−13509

5. CONCLUSIONS

The foaming properties of C_{12}-ALA, C_{12}-LEU, and C_{12}-PHE surfactants mixed with C_8OH were thoroughly investigated via surface tension and foamability experiments and complemented by all-atom detail MD simulations. The surface tension measurements revealed significant differences between the used AAS at equilibrium conditions, i.e., the highest synergistic effect was observed for the C_{12}-ALA/C_8OH system, while for C_{12}-PHE/C_8OH, the effect was antagonistic. In contrast, under dynamic conditions (foamability experiments), all studied AAS/C_8OH mixtures exhibited a spectacular synergistic effect at a wide concentration range, in comparison to the one-component systems. We connected the observed phenomenon with the hydrogen bond-mediated aggregate formation in the bulk solution. Moreover, we explained the differences between the specific AAS via the interplay of AAS−AAS and AAS-C_8OH hydrogen bond affinities.

The presented results point toward more general conclusions, which might be potentially applied to a much broader range of surfactant mixtures: (i) the molecule's hydrogen bonding affinity can be used to control the foaming properties, (ii) bulk aggregates can act as surfactant reservoirs, activated by the strong convection (mixing or flotation, and this effect can be generally described as convection-activated surface activity), (iii) surfactants with low solubility (lack of CMC) or relatively weak surface activity at the equilibrium conditions can still be considered as potentially efficient foaming additives, and (iv) molecules with considerable affinity to form hydrogen bonds, such as AAS presented here, can possibly strengthen the interactions with hydrophilic surfaces (e.g., oxide minerals) via hydrogen bonding.

The revealed discrepancy between CSC_σ and CSC_{DFA} is an additional confirmation of the crucial importance of the convection-activated surface activity in the magnitude of the synergistic effect for the studied mixed AASs and *n*-octanol solutions. Moreover, it shows that the CSC value is not universal, and in specific systems, it cannot be simply predicted from the equilibrium surface tension data. Convection-activated surface activity causes the CSC_{DFA} value to depend strongly on the foam formation dynamics (gas flow rate, foaming time, foam column height), i.e., on the parameters directly determining the rate of depletion in the AASs bulk concentration and the kinetics of the aggregates decomposition.

AUTHOR INFORMATION

Corresponding Authors

Przemyslaw B. Kowalczuk − *Department of Geoscience and Petroleum, Norwegian University of Science and Technology, 7031 Trondheim, Norway;* orcid.org/0000-0002-1432-030X; Email: przemyslaw.kowalczuk@ntnu.no

Jan Zawala − *Jerzy Haber Institute of Catalysis and Surface Chemistry, Polish Academy of Sciences, 30-239 Krakow, Poland;* orcid.org/0000-0003-4542-2226; Email: jan.zawala@ikifp.edu.pl

Authors

Mariusz Borkowski − *Jerzy Haber Institute of Catalysis and Surface Chemistry, Polish Academy of Sciences, 30-239 Krakow, Poland;* orcid.org/0000-0002-2276-2247

Piotr Batys − *Jerzy Haber Institute of Catalysis and Surface Chemistry, Polish Academy of Sciences, 30-239 Krakow, Poland;* orcid.org/0000-0002-2264-3053

Oleg M. Demchuk − *Faculty of Medicine, The John Paul II Catholic University of Lublin, 20-708 Lublin, Poland*

Complete contact information is available at: https://pubs.acs.org/10.1021/acs.iecr.3c01972

Notes

The authors declare no competing financial interest.

ACKNOWLEDGMENTS

Partial financial support from the Polish National Science Centre grant no. (2020/38/E/ST8/00173 and 2022/45/N/ST8/02307) is acknowledged with gratitude. P.B. and J.Z. acknowledge the partial financial support to the project by the statutory research fund of ICSC PAS. We gratefully acknowledge Poland's high-performance computing infrastructure PLGrid (HPC Centers: ACK Cyfronet AGH) for providing computer facilities and support within computational grant no. PLG/2023/016229.

REFERENCES

(1) Atta, D. Y.; Negash, B. M.; Yekeen, N.; Habte, A. D. A State-of-the-Art Review on the Application of Natural Surfactants in Enhanced Oil Recovery. *J. Mol. Liq.* **2021**, *321*, 114888.

(2) Tripathy, D. B.; Mishra, A.; Clark, J.; Farmer, T. S. Synthesis, chemistry, physicochemical properties and industrial applications of amino acid surfactants: A review. *C. R. Chim.* **2018**, *21*, 112−130.

(3) Liu, P.; Wu, J.; Pei, X.; Cui, Z.; Jiang, J.; Song, B.; Binks, B. P. Recyclable Surfactant Containing a Dynamic Covalent Bond and Relevant Smart Emulsions. *Green Chem.* **2022**, *24*, 7612−7621.

(4) Xu, M.; Li, Q.; Xie, M.; Jia, Y. G.; Yang, Y.; Chen, Y. Engineering Air-in-Water Emulsion as Adaptable Multifunctional Sealant. *Chem. Eng. J.* **2022**, *429*, 132200.

(5) Litauszki, K.; Gere, D.; Czigany, T.; Kmetty, Á. Environmentally Friendly Packaging Foams: Investigation of the Compostability of Poly(Lactic Acid)-Based Syntactic Foams. *Sustainable Mater. Technol.* **2023**, *35*, No. e00527.

(6) Stie, M. B.; Kalouta, K.; da Cunha, C. F. B.; Feroze, H. M.; Vetri, V.; Foderà, V. Sustainable Strategies for Waterborne Electrospinning of Biocompatible Nanofibers Based on Soy Protein Isolate. *Sustainable Mater. Technol.* **2022**, *34*, No. e00519.

(7) Lin, H.; Chen, K.; Zheng, S.; Zeng, R.; Lin, Y.; Jian, R.; Bai, W.; Xu, Y. Facile Fabrication of Natural Superhydrophobic Eleostearic Acid-SiO2@cotton Fabric for Efficient Separation of Oil/Water Mixtures and Emulsions. *Sustainable Mater. Technol.* **2022**, *32*, No. e00418.

(8) Johnson, P.; Trybala, A.; Starov, V.; Pinfield, V. J. Effect of Synthetic Surfactants on the Environment and the Potential for Substitution by Biosurfactants. *Adv. Colloid Interface Sci.* **2021**, *288*, 102340.

(9) Gallou, F.; Isley, N. A.; Ganic, A.; Onken, U.; Parmentier, M. Surfactant Technology Applied toward an Active Pharmaceutical Ingredient: More than a Simple Green Chemistry Advance. *Green Chem.* **2016**, *18*, 14−19.

(10) Tang, J.; He, J.; Xin, X.; Hu, H.; Liu, T. Biosurfactants Enhanced Heavy Metals Removal from Sludge in the Electrokinetic Treatment. *Chem. Eng. J.* **2018**, *334*, 2579−2592.

(11) Verma, S. P.; Sarkar, B. Rhamnolipid Based Micellar-Enhanced Ultrafiltration for Simultaneous Removal of Cd(II) and Phenolic Compound from Wastewater. *Chem. Eng. J.* **2017**, *319*, 131−142.

(12) Viisimaa, M.; Karpenko, O.; Novikov, V.; Trapido, M.; Goi, A. Influence of Biosurfactant on Combined Chemical−Biological Treatment of PCB-Contaminated Soil. *Chem. Eng. J.* **2013**, *220*, 352−359.

(13) *Mixed Surfactant Systems*; Masahiko, A., Ed.; Taylor & Francis eBooks, 1992. https://www.taylorfrancis.com/books/edit/10.1201/

9781420031010/mixed-surfactant-systems-masahiko-abe (accessed Feb 27, 2023).
(14) Liang, X.; Zhang, M.; Guo, C.; Abel, S.; Yi, X.; Lu, G.; Yang, C.; Dang, Z. Competitive Solubilization of Low-Molecular-Weight Polycyclic Aromatic Hydrocarbons Mixtures in Single and Binary Surfactant Micelles. *Chem. Eng. J.* **2014**, *244*, 522−530.
(15) Chiwetelu, C. I.; Hornof, V.; Neale, G. H.; George, A. E. Use of Mixed Surfactants to Improve the Transient Interfacial Tension Behaviour of Heavy Oil/Alkaline Systems. *Can. J. Chem. Eng.* **1994**, *72*, 534−540.
(16) Wiertel-Pochopien, A.; Batys, P.; Zawala, J.; Kowalczuk, P. B. Synergistic Effect of Binary Surfactant Mixtures in Two-Phase and Three-Phase Systems. *J. Phys. Chem. B* **2021**, *125*, 3855−3866.
(17) Khan, A.; Marques, E. F. Synergism and Polymorphism in Mixed Surfactant Systems. *Curr. Opin. Colloid Interface Sci.* **1999**, *4*, 402−410.
(18) Polowczyk, I.; Kruszelnicki, M.; Kowalczuk, P. B. Oil Agglomeration of Metal-Bearing Shale in the Presence of Mixed Cationic-Anionic Surfactants. *Physicochem. Probl. Miner. Process.* **2018**, *54*, 1052−1059.
(19) Rangsunvigit, P.; Imsawatgul, P.; Na-ranong, N.; O'Haver, J. H.; Chavadej, S. Mixed Surfactants for Silica Surface Modification by Admicellar Polymerization Using a Continuous Stirred Tank Reactor. *Chem. Eng. J.* **2008**, *136*, 288−294.
(20) Lin, S. Y. A.; Lin, Y. Y.; Chen, E. M.; Hsu, C. T.; Kwan, C. C. A Study of the Equilibrium Surface Tension and the Critical Micelle Concentration of Mixed Surfactant Solutions. *Langmuir* **1999**, *15*, 4370−4376.
(21) Wang, Y.; Jiang, Y.; Geng, T.; Ju, H.; Duan, S. Synthesis, Surface/Interfacial Properties, and Biological Activity of Amide-Based Gemini Cationic Surfactants with Hydroxyl in the Spacer Group. *Colloids Surf., A* **2019**, *563*, 1−10.
(22) Bera, A.; Ojha, K.; Mandal, A. Synergistic Effect of Mixed Surfactant Systems on Foam Behavior and Surface Tension. *J. Surfactants Deterg.* **2013**, *16*, 621−630.
(23) Stellner, K. L.; Scamehorn, J. F. Surfactant Precipitation in Aqueous Solutions Containing Mixtures of Anionic and Nonionic Surfactants. *J. Am. Oil Chem. Soc.* **1986**, *63*, 566−574.
(24) Kume, G.; Gallotti, M.; Nunes, G. Review on Anionic/Cationic Surfactant Mixtures. *J. Surfactants Deterg.* **2008**, *11*, 1−11.
(25) Stellner, K. L.; Amante, J. C.; Scamehorn, J. F.; Harwell, J. H. Precipitation Phenomena in Mixtures of Anionic and Cationic Surfactants in Aqueous Solutions. *J. Colloid Interface Sci.* **1988**, *123*, 186−200.
(26) Ramezani, M.; Lashkarbolooki, M.; Abedini, R. Experimental Investigation of Different Characteristics of Crude Oil on the Interfacial Activity of Anionic, Cationic and Nonionic Surfactants Mixtures. *J. Pet. Sci. Eng.* **2022**, *214*, 110485.
(27) Poorsargol, M.; Alimohammadian, M.; Sohrabi, B.; Dehestani, M. Dispersion of Graphene Using Surfactant Mixtures: Experimental and Molecular Dynamics Simulation Studies. *Appl. Surf. Sci.* **2019**, *464*, 440−450.
(28) Bordes, R.; Holmberg, K. Amino Acid-Based Surfactants − Do They Deserve More Attention? *Adv. Colloid Interface Sci.* **2015**, *222*, 79−91.
(29) Guo, J.; Sun, L.; Zhang, F.; Sun, B.; Xu, B.; Zhou, Y. Review: Progress in Synthesis, Properties and Application of Amino Acid Surfactants. *Chem. Phys. Lett.* **2022**, *794*, 139499.
(30) Qiao, W.; Qiao, Y. The Relationship Between the Structure and Properties of Amino Acid Surfactants Based on Glycine and Serine. *J. Surfactants Deterg.* **2013**, *16*, 821−828.
(31) Borkowski, M.; Orvalho, S.; Warszyński, P.; Demchuk, O. M.; Jarek, E.; Zawala, J. Experimental and Theoretical Study of Adsorption of Synthesized Amino Acid Core Derived Surfactants at an Air/Water Interface. *Phys. Chem. Chem. Phys.* **2022**, *24*, 3854−3864.
(32) Miroslaw, B.; Demchuk, O. M.; Luboradzki, R.; Tyszczuk-Rotko, K. Low-Molecular-Weight Organogelators Based on N-Dodecanoyl-L-Amino Acids—Energy Frameworks and Supramolecular Synthons. *Materials* **2023**, *16*, 702.
(33) Berendsen, H. J. C.; van der Spoel, D.; van Drunen, R. GROMACS: A message-passing parallel molecular dynamics implementation. *Comput. Phys. Commun.* **1995**, *91*, 43−56.
(34) Lindahl, E.; Hess, B.; van der Spoel, D. GROMACS 3.0: A Package for Molecular Simulation and Trajectory Analysis. *J. Mol. Model.* **2001**, *7*, 306−317.
(35) MacKerell, A. D.; Bashford, D.; Bellott, M.; Dunbrack, R. L.; Evanseck, J. D.; Field, M. J.; Fischer, S.; Gao, J.; Guo, H.; Ha, S.; Joseph-McCarthy, D.; Kuchnir, L.; Kuczera, K.; Lau, F. T. K.; Mattos, C.; Michnick, S.; Ngo, T.; Nguyen, D. T.; Prodhom, B.; Reiher, W. E.; Roux, B.; Schlenkrich, M.; Smith, J. C.; Stote, R.; Straub, J.; Watanabe, M.; Wiórkiewicz-Kuczera, J.; Yin, D.; Karplus, M. All-Atom Empirical Potential for Molecular Modeling and Dynamics Studies of Proteins. *J. Phys. Chem. B* **1998**, *102*, 3586−3616.
(36) Yazhgur, P.; Vierros, S.; Hannoy, D.; Sammalkorpi, M.; Salonen, A. Surfactant Interactions and Organization at the Gas-Water Interface (CTAB with Added Salt). *Langmuir* **2018**, *34*, 1855−1864.
(37) Jo, S.; Kim, T.; Iyer, V. G.; Im, W. CHARMM-GUI: A Web-Based Graphical User Interface for CHARMM. *J. Comput. Chem.* **2008**, *29*, 1859−1865.
(38) Brooks, B. R.; Brooks, C. L.; Mackerell, A. D.; Nilsson, L.; Petrella, R. J.; Roux, B.; Won, Y.; Archontis, G.; Bartels, C.; Boresch, S.; Caflisch, A.; Caves, L.; Cui, Q.; Dinner, A. R.; Feig, M.; Fischer, S.; Gao, J.; Hodoscek, M.; Im, W.; Kuczera, K.; Lazaridis, T.; Ma, J.; Ovchinnikov, V.; Paci, E.; Pastor, R. W.; Post, C. B.; Pu, J. Z.; Schaefer, M.; Tidor, B.; Venable, R. M.; Woodcock, H. L.; Wu, X.; Yang, W.; York, D. M.; Karplus, M. CHARMM: The Biomolecular Simulation Program. *J. Comput. Chem.* **2009**, *30*, 1545−1614.
(39) Lee, J.; Cheng, X.; Swails, J. M.; Yeom, M. S.; Eastman, P. K.; Lemkul, J. A.; Wei, S.; Buckner, J.; Jeong, J. C.; Qi, Y.; Jo, S.; Pande, V. S.; Case, D. A.; Brooks, C. L.; MacKerell, A. D.; Klauda, J. B.; Im, W. CHARMM-GUI Input Generator for NAMD, GROMACS, AMBER, OpenMM, and CHARMM/OpenMM Simulations Using the CHARMM36 Additive Force Field. *J. Chem. Theory Comput.* **2016**, *12*, 405−413.
(40) Vanommeslaeghe, K.; Hatcher, E.; Acharya, C.; Kundu, S.; Zhong, S.; Shim, J.; Darian, E.; Guvench, O.; Lopes, P.; Vorobyov, I.; Mackerell, A. D. CHARMM General Force Field: A Force Field for Drug-like Molecules Compatible with the CHARMM All-Atom Additive Biological Force Fields. *J. Comput. Chem.* **2009**, *31*, 671−690.
(41) Jorgensen, W. L.; Chandrasekhar, J.; Madura, J. D.; Impey, R. W.; Klein, M. L. Comparison of Simple Potential Functions for Simulating Liquid Water. *J. Chem. Phys.* **1983**, *79*, 926−935.
(42) Bussi, G.; Donadio, D.; Parrinello, M. Canonical Sampling through Velocity Rescaling. *J. Chem. Phys.* **2007**, *126*, 014101.
(43) Essmann, U.; Perera, L.; Berkowitz, M. L.; Darden, T.; Lee, H.; Pedersen, L. G. A Smooth Particle Mesh Ewald Method. *J. Chem. Phys.* **1995**, *103*, 8577−8593.
(44) Yeh, I. C.; Berkowitz, M. L. Ewald Summation for Systems with Slab Geometry. *J. Chem. Phys.* **1999**, *111*, 3155−3162.
(45) Hess, B.; Bekker, H.; Berendsen, H. J. C.; Fraaije, J. G. E. M. LINCS: A Linear Constraint Solver for Molecular Simulations. *J. Comput. Chem.* **1997**, *18*, 1463−1472.
(46) Miyamoto, S.; Kollman, P. A. Settle: An Analytical Version of the SHAKE and RATTLE Algorithm for Rigid Water Models. *J. Comput. Chem.* **1992**, *13*, 952−962.
(47) Humphrey, W.; Dalke, A.; Schulten, K. VMD: Visual Molecular Dynamics. *J. Mol. Graph.* **1996**, *14*, 33−38.
(48) Martinez, L.; Andrade, R.; Birgin, E. G.; Martínez, J. M. PACKMOL: A Package for Building Initial Configurations for Molecular Dynamics Simulations. *J. Comput. Chem.* **2009**, *30*, 2157−2164.
(49) Zawala, J.; Wiertel-Pochopien, A.; Larsen, E.; Kowalczuk, P. B. Synergism between Cationic Alkyltrimethylammonium Bromides (C_nTAB) and Nonionic *n*-Octanol in the Foamability of Their Mixed Solutions. *Ind. Eng. Chem. Res.* **2020**, *59*, 1159−1167.

(50) Lunkenheimer, K.; Malysa, K.; Winsel, K.; Geggel, K.; Siegel, S. Novel Method and Parameters for Testing and Characterization of Foam Stability. *Langmuir* **2010**, *26*, 3883−3888.
(51) Kim, I. J.; Park, J. G.; Han, Y. H.; Kim, S. Y.; Shackelford, J. F.; Kim, I. J.; Park, J. G.; Han, Y. H.; Kim, S. Y.; Shackelford, J. F. Wet Foam Stability from Colloidal Suspension to Porous Ceramics: A Review. *J. Korean Ceram. Soc.* **2019**, *56*, 211−232.

https://doi.org/10.1021/acs.iecr.3c01972
Ind. Eng. Chem. Res. 2023, 62, 13498−13509